Proceedings of CHT-15
ICHMT International Symposium on Advances in Computational Heat Transfer

May 25-29, 2015, Rutgers University, Piscataway, USA

CHT-15-237

FORM-DRAG EFFECTS IN THE CONVECTIVE INSTABILITY OF PARALLEL FLOW IN A HORIZONTAL POROUS LAYER WITH UNIFORM WALL HEATING

A. Barletta[*,§], D. A. S. Rees[**]
[*]Dept. of Industrial Engineering, Alma Mater Studiorum Università di Bologna, Italy
[**]Dept. of Mechanical Engineering, University of Bath, UK
[§]Correspondence author. Fax: +39 051 2093296 Email: antonio.barletta@unibo.it

ABSTRACT The instability of through flow in a horizontal porous channel with uniformly heated boundary walls is investigated. The analysis is based on the solution of the linearised perturbation equations expressing the local mass and energy balances, as well as the momentum balance modelled according to Darcy-Forchheimer's law. The neutral stability data are obtained in terms of the dimensionless governing parameters, namely the Darcy-Rayleigh number, the Péclet number, and the form-drag parameter.

INTRODUCTION

The analysis of forced or mixed convection in porous channels is of primary interest for applications involving heat transfer enhancement and for the design of innovative heat exchangers. Materials typically involved in these applications are metal foams. In fact, the high thermal conductivity of these media, together with the high contact area between the solid and the fluid, serves to enhance significantly the heat transfer rates. Modelling flow in porous media implies that form-drag effects be included whenever the permeability-based Reynolds number is close to 1 or larger (Nield and Bejan, 2013). When the form-drag term is included, the resulting local momentum balance becomes intrinsically nonlinear due to the quadratic term in the seepage velocity. The importance of form-drag in the heat transfer of porous media flows is not only restricted to cases of forced convection, but it may arise also for a mixed convection regime. A typical situation is that arising when a steady fluid flow takes place in a horizontal porous layer bounded by impermeable walls kept at different temperatures. Under conditions of heating from below, a convective instability may arise when the Rayleigh number, R, becomes sufficiently large (Prats, 1966). On taking into account the form-drag effect, the critical value of R is sensibly influenced by the form-drag dimensionless parameter, G (Rees, 1997). The analysis carried out by Prats (1966), based on the linear Darcy's law for momentum transfer, is recovered in the limit $G \to 0$. Rees (1997) was able to prove that the form-drag effect yields a stabilisation of the basic flow. In other words, when $G > 0$, the critical Rayleigh number for the onset of the instability is larger than in the limit of validity of Darcy's law, $G \to 0$. Further studies on this topic were performed by Dodgson and Rees (2013), who considered the effect of the time derivative term in Darcy's law, and by Rees and Mojtabi (2013), who assumed a non-negligible thickness of the boundary conducting walls.

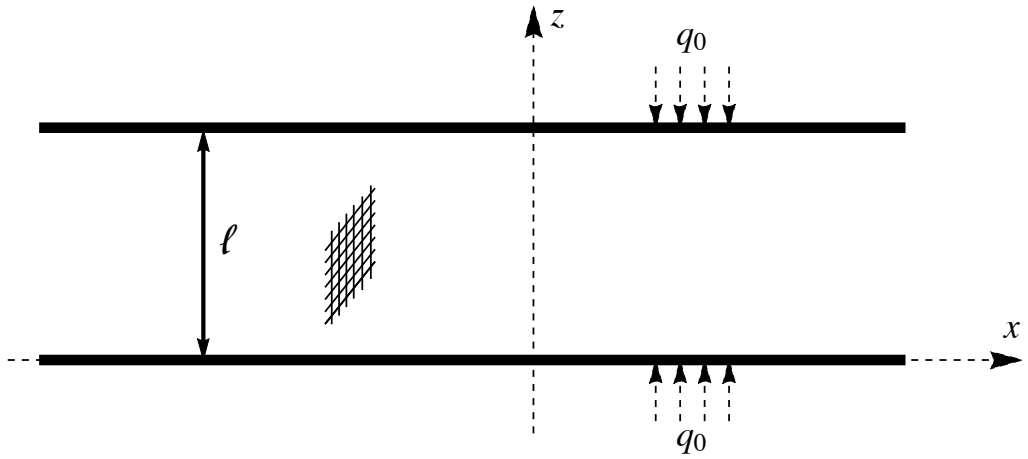

Figure 1. Porous channel with horizontal throughflow

The study carried out by Rees (1997) is relative to a case where the basic temperature gradient is purely vertical, meaning that the heat supplied from the lower boundary is entirely dissipated through the upper boundary. Different conditions of mixed convection arise when the basic temperature gradient is inclined to the vertical. This is the case when the heat supplied and dissipated through the walls is unbalanced at a given streamwise position so that a net fluid heating or cooling occurs downstream. This situation was investigated by Barletta (2012), with reference to the stationary mixed convection in a horizontal porous channel bounded by a pair of symmetrically heated impermeable walls. In this study, the Péclet number, P, associated with the basic throughflow could not be set to zero without inducing an unsteady behaviour in the system. On the other hand, the steady mixed convection regime is ensured by the imposed horizontal throughflow which convects downstream the heat supplied to the walls. The critical Rayleigh number for the onset of the thermal instability depends on P. Barletta (2012) proved that no instability takes place when $P < 19.1971$. Further developments closely related to the analysis presented in Barletta (2012) were carried out in other papers (Barletta et al., 2013; Barletta, 2013).
The aim of this paper is to extend the analysis developed by Barletta (2012), by investigating the effects of the form-drag term in the local momentum balance equation. The form-drag effect is expected to be twofold: it influences the basic flow solution, and it produces a change in the eigenvalue problem formulation of the linear stability analysis. The linear stability analysis will be carried out numerically, by employing an explicit Runge-Kutta method combined with the shooting method.

GOVERNING EQUATIONS

Let us consider a horizontal parallel plane channel with thickness ℓ bounded by impermeable rigid walls kept at a uniform heat flux q_0. The channel (see Fig. 1) contains a fluid saturated porous medium considered as homogeneous and isotropic. The $x-$axis and $y-$axis are horizontal, while the $z-$axis is oriented vertically so that the gravitational acceleration is $\mathbf{g} = -g\,\mathbf{e}_z$. Here, g is the modulus of $\mathbf{g}$ and $\mathbf{e}_z$ is the unit vector along the $z-$axis. The seepage flow due to the buoyancy and to an imposed horizontal pressure gradient is modelled under the following assumptions:

- Form-drag effect is non-negligible, so that Darcy-Forchheimer's law holds;
- The Oberbeck–Boussinesq approximation can be applied;
- The porous medium is isotropic and homogeneous;
- A condition of local thermal equilibrium between the solid phase and the fluid phase holds;
- The effect of viscous dissipation can be neglected.

These assumptions are reasonable when the flow rates are sufficiently high for the form-drag effect to be

important, but not so intense as to suppress the contribution of buoyancy, or to induce a sensible effect of viscous heating. Flow in highly permeable media, such as the metal foams, is prone to display this behaviour.
According to the above stated assumptions, the governing equations can be written in a dimensionless form as

$$\boldsymbol{\nabla}\cdot\mathbf{u} = 0, \tag{1a}$$

$$\boldsymbol{\nabla}\times\left[\left(1+\xi|\mathbf{u}|\right)\mathbf{u}\right] = \boldsymbol{\nabla}\times\left(T\mathbf{e}_z\right), \tag{1b}$$

$$\frac{\partial T}{\partial t} + \mathbf{u}\cdot\boldsymbol{\nabla}T = \nabla^2 T, \tag{1c}$$

with the boundary conditions

$$\begin{aligned} z = 0: \qquad & w = 0, \qquad \frac{\partial T}{\partial z} = -R, \\ z = 1: \qquad & w = 0, \qquad \frac{\partial T}{\partial z} = R. \end{aligned} \tag{2}$$

We note that the velocity boundary conditions are limited to the impermeability constraint, while no-slip conditions are not allowed within Darcy-Forchheimer's model. Here, the dimensionless coordinates, time, velocity field and temperature field have been denoted as: $\mathbf{x} = (x, y, z)$, t, $\mathbf{u} = (u, v, w)$, and T, respectively. Eq. (1b) is obtained by applying the curl operator to both sides of the local momentum balance equation, so that the pressure gradient contribution disappears.
The dimensionless variables are defined as

$$\begin{aligned} (x^*, y^*, z^*)\,\frac{1}{\ell} &= (x, y, z), \qquad t^*\,\frac{\alpha}{\sigma\ell^2} = t, \\ (u^*, v^*, w^*)\,\frac{\ell}{\alpha} &= (u, v, w), \qquad (T^* - T_0)\,\frac{g\beta K\ell}{\nu\alpha} = T, \end{aligned} \tag{3}$$

where the starred symbols denote the dimensional coordinates, time, velocity field and temperature field, while T_0 is the average fluid temperature within the channel. The symbol K denotes the permeability; α is the average thermal diffusivity; β is the thermal expansion coefficient of the fluid; ν is the kinematic viscosity of the fluid. The dimensionless quantity σ is the heat capacity ratio, *viz.* the ratio between the average volumetric heat capacity of the fluid–saturated porous medium and the volumetric heat capacity of the fluid.
The Darcy–Rayleigh number R and the form-drag parameter ξ are defined as

$$R = \frac{g\beta q_0 K\,\ell^2}{\nu\alpha\lambda}, \qquad \xi = \frac{c_f\alpha\,\sqrt{K}}{\nu\ell}, \tag{4}$$

where λ is the average thermal conductivity, and c_f is the form-drag coefficient (Nield and Bejan, 2013). Given that K is unlikely to be larger than $10^{-4}\,\mathrm{cm}^2$ in practical cases (Nield and Bejan, 2013), the parameter ξ is expected to be reasonably smaller than 10^{-2}, if $\ell \cong 1\,\mathrm{cm}$ or larger. Obviously, one may consider channels with a smaller thickness, but then the buoyancy effect would hardly be significant.
The uniform wall heat flux q_0, and hence the Darcy–Rayleigh number R, can be either positive or negative. If $q_0 > 0$ ($R > 0$), the fluid saturated porous medium is symmetrically heated through the boundary walls. If $q_0 < 0$ ($R < 0$), the fluid saturated porous medium is symmetrically cooled through the boundary walls. These cases are modelled by the Neumann boundary conditions on T, Eq. (2).

THE BASIC MIXED CONVECTION FLOW

A stationary solution of Eqs. (1) and (2) can be found, given by

$$\mathbf{u}_b = U(z)\mathbf{e}_x, \qquad \boldsymbol{\nabla} T_b = C\mathbf{e}_x + Q(z)\,\mathbf{e}_z, \tag{5}$$

where constant C and functions $U(z)$, $Q(z)$ are determined from Eqs. (1) and (2). In particular, Eq. (2) is satisfied if $Q(0) = -R$ and $Q(1) = R$. Then, Eq. (1c) implies that

$$Q(z) = -R + C\int_0^z U(\zeta)\,d\zeta, \tag{6}$$

where ζ is a dummy integration variable. Let us introduce a Péclet number for the average flow, so that

$$P = \int_0^1 U(\zeta)\,d\zeta. \tag{7}$$

Hence, the boundary condition $Q(1) = R$ is satisfied if

$$C = 2R/P \tag{8}$$

As it can be deduced from Eq. (5), C represents the linear growth of temperature along the $x-$direction. This growth parameter is inversely proportional to P, so that it becomes singular when $P \to 0$. In fact, $P \to 0$ means a vanishing flow rate along the channel. In this limiting case, no stationary solution compatible with the boundary conditions (2) is allowed. The flow is considered, without loss of generality, to be directed along the positive $x-$axis, meaning $P > 0$.
Equation (1b) yields

$$\left[1 + \xi|U(z)|\right] U(z) = A - \frac{2R}{P}\,z, \tag{9}$$

where A is a constant. We will carry out the forthcoming analysis by assuming the basic flow to be unidirectional, *viz.* $U(z) > 0$ for every $z \in [0,1]$ or equivalently $A > 2R/P$. This condition is expected to be satisfied when the Péclet number is sufficiently large. The assumption of a fairly large P is reasonable given that we aim to explore the effects of the form-drag contribution to the momentum balance. On inspecting Eqs. (7) and (9), these effects are expected to be important when $\xi P \sim O(1)$ or larger. Thus, due to the order of magnitude of ξ discussed in the previous section, one may easily devise that P must be large for the form-drag effect to modify significantly the basic solution. Equation (9), on assuming $U(z) > 0$, leads to the expression

$$U(z) = \frac{1}{2\xi}\left[\sqrt{4\xi\left(A - \frac{2R}{P}\,z\right) + 1} - 1\right], \tag{10}$$

so that Eq. (6) yields

$$Q(z) = -R - \frac{R\,z}{\xi P} + \frac{1}{12P\xi^2}\left[8\xi R z\,\sqrt{4A\xi - \frac{8\xi R z}{P} + 1}\right. \\ \left. +\; P(4A\xi+1)\left(\sqrt{4A\xi+1} - \sqrt{4A\xi - \frac{8\xi R z}{P} + 1}\right)\right]. \tag{11}$$

The constant A can be determined by imposing the boundary condition $Q(1) = R$. Hence, Eq. (11) leads to the algebraic equation

$$2R = -\frac{R}{\xi P} + \frac{1}{12P\xi^2}\left[8\xi R\,\sqrt{4A\xi - \frac{8\xi R}{P} + 1}\right. \\ \left. +\; P(4A\xi+1)\left(\sqrt{4A\xi+1} - \sqrt{4A\xi - \frac{8\xi R}{P} + 1}\right)\right], \tag{12}$$

which can be solved with prescribed values of the input parameters (ξ, R, P).
In a regime where the form-drag effect is negligible, namely $\xi \to 0$, Eqs. (10)–(12) provide the asymptotic expressions

$$A \cong P + \frac{R}{P}, \tag{13a}$$

$$U(z) \cong A - \frac{2R}{P}\,z = P - \frac{2R}{P}\left(z - \frac{1}{2}\right), \tag{13b}$$

$$Q(z) \cong -R + \frac{2AR}{P}\,z - \frac{2R^2}{P^2}\,z^2 = -R + 2R\left(1 + \frac{R}{P^2}\right)z - \frac{2R^2}{P^2}\,z^2. \tag{13c}$$

Equations (5) and (13) are in perfect agreement with the basic solution found for the case of Darcy's model by Barletta (2012).
Another sensible asymptotic regime is $P \gg 1$, namely the limiting case of a basic forced convection flow. In this regime, we have a drastic simplification of Eqs. (10)–(12), leading to

$$U(z) \cong P, \tag{14a}$$

$$Q(z) \cong 2R\left(z - \frac{1}{2}\right). \tag{14b}$$

As a result, in the asymptotic regime $P \gg 1$, the basic solution (5) becomes independent of the form-drag parameter ξ. In other words, the basic solution with $P \gg 1$ is exactly the same as that predicted by employing Darcy's law. This result is only apparently surprising. In fact, when the impressed throughflow is very intense, the non-uniformity in the velocity profile due to effect of buoyancy is almost completely suppressed and, hence, Eq. (14a) follows. Therefore, Eq. (14b) is a direct consequence of Eqs. (6) and (14a). In practice, the asymptotic behaviour with $P \gg 1$ implies that the form-drag effect influences the basic flow just through the relationship between the average basic velocity and the pressure drop imposed across the channel.

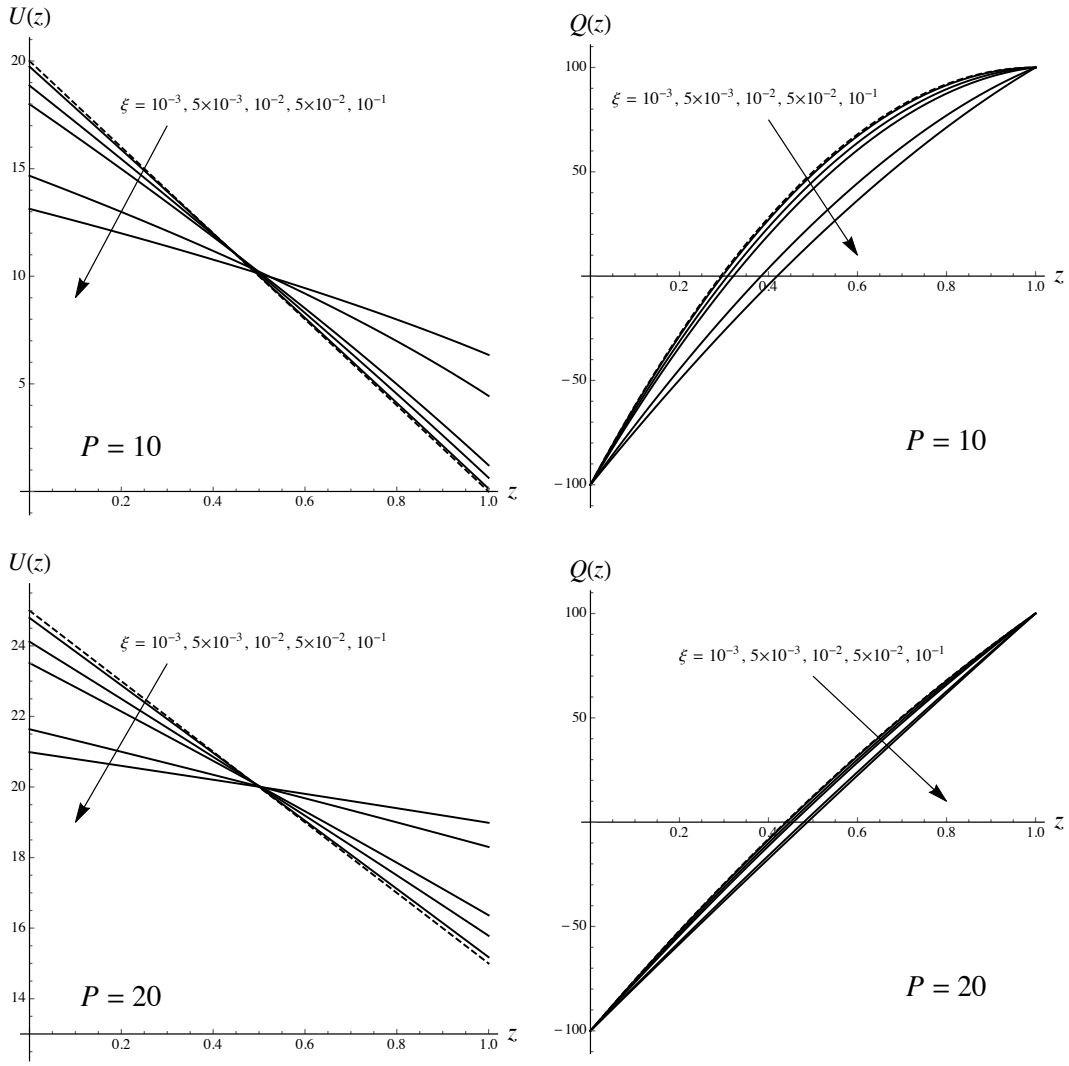

Figure 2. Basic flow: velocity profiles, $U(z)$, and heat flux profiles, $Q(z)$, when $R = 100$ and P is either 10 or 20. The dashed lines correspond to the limit of Darcy's law, $\xi \to 0$

Figure 2 illustrates the influence of the form-drag parameter ξ on the velocity and heat flux distributions, $U(z)$ and $Q(z)$, in the basic flow. The case where $R = 100$ has been considered with either $P = 10$ or $P = 20$. A wide range of ξ, from 10^{-3} to 10^{-1}, has been considered, and a comparison with the trends relative to Darcy's limiting case $\xi \to 0$ (dashed lines) can be made. One may see that the differences between the case $\xi = 10^{-3}$ and the limiting case $\xi \to 0$ are very small. Moreover, the effect of ξ becomes weaker when P is larger. The latter feature is consistent with the characteristic of the basic solution in the asymptotic case $P \gg 1$, where the effect of ξ on the basic solution becomes negligible. Another aspect of the basic solution, displayed in Fig. 2, is that the asymptotic behaviour for $P \gg 1$ is closely approached for smaller values of P the higher is the value of ξ. Roughly speaking, the form-drag effect accelerates the transition from mixed to forced convection as P increases. We finally mention that the asymmetry of the velocity and temperature profiles is a consequence of the buoyancy force acting along the $z-$axis. When the buoyancy effect becomes negligible, *viz.* when $P \gg 1$, the asymmetry disappears.

STABILITY ANALYSIS

We now test the stability of the basic state, given by Eqs. (5), (10) and (11), by expressing the perturbed velocity and temperature as

$$\mathbf{u} = \mathbf{u}_b + \tilde{\mathbf{u}}, \qquad \boldsymbol{\nabla} T = \boldsymbol{\nabla} T_b + \boldsymbol{\nabla} \tilde{T}, \tag{15}$$

where $\tilde{\mathbf{u}} = (\tilde{u}, \tilde{v}, \tilde{w})$ and $\tilde{T}$ are the perturbation fields. Consistently with a linear stability analysis, we will assume the perturbation fields to be very small with respect to the basic flow fields $\mathbf{u}_b$ and T_b. Therefore, nonlinear terms in the perturbation fields will be considered as negligible in Eqs. (1) and (2) and we can write the governing equations and boundary conditions as

$$\frac{\partial \tilde{u}}{\partial x} + \frac{\partial \tilde{v}}{\partial y} + \frac{\partial \tilde{w}}{\partial z} = 0, \tag{16a}$$

$$\xi U'(z)\tilde{v} + [\xi U(z) + 1]\left(\frac{\partial \tilde{v}}{\partial z} - \frac{\partial \tilde{w}}{\partial y}\right) = -\frac{\partial \tilde{T}}{\partial y}, \tag{16b}$$

$$2\xi U'(z)\tilde{u} + [2\xi U(z) + 1]\frac{\partial \tilde{u}}{\partial z} - [\xi U(z) + 1]\frac{\partial \tilde{w}}{\partial x} = -\frac{\partial \tilde{T}}{\partial x}, \tag{16c}$$

$$[\xi U(z) + 1]\frac{\partial \tilde{v}}{\partial x} - [2\xi U(z) + 1]\frac{\partial \tilde{u}}{\partial y} = 0, \tag{16d}$$

$$\frac{\partial \tilde{T}}{\partial t} + \frac{2R}{P}\,\tilde{u} + Q(z)\tilde{w} + U(z)\,\frac{\partial \tilde{T}}{\partial x} = \frac{\partial^2 \tilde{T}}{\partial x^2} + \frac{\partial^2 \tilde{T}}{\partial y^2} + \frac{\partial^2 \tilde{T}}{\partial z^2}, \tag{16e}$$

$$z = 0, 1: \qquad \tilde{w} = 0, \qquad \frac{\partial \tilde{T}}{\partial z} = 0, \tag{16f}$$

where primes denote derivatives with respect to z.

Longitudinal Rolls The perturbation fields $(\tilde{u}, \tilde{v}, \tilde{w})$ and $\tilde{T}$ are expressed in terms of normal modes. In the limiting case of Darcy's flow, investigated by Barletta (2012), the most unstable modes are the longitudinal rolls. These special normal modes are such that

$$\tilde{u} = 0, \quad \tilde{v} = \tilde{v}(y, z, t), \quad \tilde{w} = \tilde{w}(y, z, t), \quad \tilde{T} = \tilde{T}(y, z, t). \tag{17}$$

In other words, they are invariant along the flow direction. For longitudinal rolls, Eqs. (16c) and (16d) are identically satisfied. Moreover, we can simplify Eqs. (16) by defining a stream function $\tilde{\psi}$ which allows us to identically satisfy Eq. (16a), namely

$$\tilde{v} = \frac{\partial \tilde{\psi}}{\partial z}, \quad \tilde{w} = -\frac{\partial \tilde{\psi}}{\partial y}. \tag{18}$$

Thus, Eqs. (16b), (16e) and (16f) yield

$$\xi U'(z)\,\frac{\partial\tilde{\psi}}{\partial z}+[\xi U(z)+1]\left(\frac{\partial^2\tilde{\psi}}{\partial y^2}+\frac{\partial^2\tilde{\psi}}{\partial z^2}\right)=-\frac{\partial\tilde{T}}{\partial y}, \tag{19a}$$

$$\frac{\partial\tilde{T}}{\partial t}-Q(z)\,\frac{\partial\tilde{\psi}}{\partial y}=\frac{\partial^2\tilde{T}}{\partial y^2}+\frac{\partial^2\tilde{T}}{\partial z^2}, \tag{19b}$$

$$z=0,1: \qquad \tilde{\psi}=0, \qquad \frac{\partial\tilde{T}}{\partial z}=0. \tag{19c}$$

We express $\tilde{\psi}$ and $\tilde{T}$ as plane waves, namely

$$\tilde{\psi}=f(z)\,e^{iky}\,e^{\eta t}, \quad \tilde{T}=ih(z)\,e^{iky}\,e^{\eta t}, \tag{20}$$

where k is the wavenumber and η is a a complex quantity, $\eta=s-i\omega$, such that s is the growth-rate parameter and ω is the angular frequency. The sign of s denotes instability, if positive, and stability, if negative. The parametric condition for the onset of instability is defined by the locus $s=0$, *viz.* the neutral stability condition.
Substitution of Eq. (20) into Eqs. (19) yields the stability eigenvalue problem,

$$[\xi U(z)+1]\left(f''-k^2f\right)+\xi U'(z)f'-kh=0, \tag{21a}$$

$$h''-\left(k^2+\eta\right)h+kQ(z)f=0, \tag{21b}$$

$$z=0,1: \qquad f=0, \qquad h'=0. \tag{21c}$$

The Asymptotic Regime of Darcy's Flow When $\xi\to 0$, the form-drag effect vanishes and the local momentum balance equation is given by Darcy's law. In this regime, the basic flow state is described by Eqs. (5) and (13). Then, Eqs. (21) are simplified to

$$f''-k^2f-kh=0, \tag{22a}$$

$$h''-\left(k^2+\eta\right)h-k\left[R-2R\left(1+\frac{R}{P^2}\right)z+\frac{2R^2}{P^2}\,z^2\right]f=0, \tag{22b}$$

$$z=0,1: \qquad f=0, \qquad h'=0. \tag{22c}$$

The eigenvalue problem (22) coincides with that obtained and analysed by Barletta (2012).

The Asymptotic Regime of Large Péclet Numbers If we assume $P\gg 1$, the basic flow solution tends to assume a simplified form given by Eqs. (5) and (14). Hence, in this asymptotic case, Eqs. (21) can be written as

$$f''-k^2f-k\theta=0, \tag{23a}$$

$$\theta''-\left(k^2+\eta\right)\theta+2\,\frac{R}{\xi P+1}\,k\left(z-\frac{1}{2}\right)f=0, \tag{23b}$$

$$z=0,1: \qquad f=0, \qquad \theta'=0, \tag{23c}$$

Table 1
Longitudinal modes with $k = 3$, $P = 25$ and $\xi = 10^{-2}$: comparison between the neutral stability values of (γ, R, A) obtained by a fixed step-size Runge-Kutta solver having gradually decreasing step-size, δz, with an adaptive step-size Runge-Kutta solver

δz	γ	R	A
0.100	-0.51618370035	198.32080320	39.276216792
0.090	-0.51624389332	198.22989554	39.272494750
0.080	-0.51628680365	198.16444685	39.269815102
0.070	-0.51631709317	198.11811999	39.267918366
0.060	-0.51633723170	198.08721744	39.266653145
0.050	-0.51634968025	198.06805117	39.265868436
0.040	-0.51635665445	198.05727894	39.265427399
0.030	-0.51635999463	198.05209903	39.265215322
0.020	-0.51636124131	198.05015887	39.265135888
0.010	-0.51636153026	198.04970754	39.265117410
0.005	-0.51636154837	198.04967918	39.265116249
0.001	-0.51636154957	198.04967729	39.265116172
adaptive	-0.51636154710	198.04968016	39.265116289

where we have rescaled the eigenfunction h, so that

$$\theta = \frac{h}{\xi P + 1}. \tag{24}$$

Equation (23) has a direct physical interpretation. If we denote by $R_0(k)$ the neutral stability function for Darcy's flow, $\xi = 0$, and with $R(k)$ the neutral stability function for a given $\xi > 0$, then we have

$$R(k) = (\xi P + 1)\, R_0(k). \tag{25}$$

Equation (25) means that the form-drag effect is stabilising as $R(k) > R_0(k)$ for every $\xi > 0$ and $P > 0$. We recall that a stabilising effect of form-drag has been found also in the analysis of Prats problem (Prats, 1966) carried out by Rees (1997).

Numerical Method A solution of the eigenvalue problem (21) can be sought by taking $\eta = 0$, which means simultaneously $s = 0$ (neutral stability condition) and $\omega = 0$. The possibility to solve numerically Eqs. (21) for non-travelling modes ($\omega = 0$) is a consequence of Eqs. (21) having real coefficients except for η itself. The solution is to be found numerically since the differential equations have variable coefficients.
First, the eigenvalue problem must be artificially turned into an initial value problem by introducing the extra parameter, γ. In other words, the boundary conditions at $z = 0$, Eq. (21c), are extended to provide a complete set of initial conditions, namely

$$f(0) = 0, \quad f'(0) = \gamma, \quad h(0) = 1, \quad h'(0) = 0. \tag{26}$$

The extra parameter γ is unknown a priori, while the condition $h(0) = 1$ is legitimate due to the scale invariance of the eigenfunction pair (f, h) in Eqs. (21). In fact, the differential equations, Eqs. (21a) and (21b), are homogeneous and the boundary conditions, Eq. (21c), are homogeneous as well. The numerical solution of Eqs. (21a), (21b) and (26) can be carried out by employing an explicit fourth-order Runge-Kutta solver. The parameters (k, P, ξ) must be prescribed, and guess-values of (R, γ, A) must be assigned. Then a shooting method, based on the Newton-Raphson technique to find iteratively a solution of algebraic equations, can be employed to solve the target conditions at $z = 1$ given by Eq. (21c), together with Eq. (12), namely

$$f(1) = 0, \quad h'(1) = 0, \quad Q(1) = R. \tag{27}$$

The solution of these three equations provides the numerical values of the three parameters γ, R and A. For every input data (P, ξ), one can record the pairs (k, R) obtained numerically in order to display graphically the neutral stability curve.
We have tested the whole procedure by comparing a fixed step-size Runge-Kutta solver with gradually decreasing step-size, δz, with an adaptive step-size Runge-Kutta solver. The test case is with $k = 3$, $P = 25$ and $\xi = 10^{-2}$, and numerical results for (γ, R, A) are reported in Table 1. The convergence of the data, as δz decreases, is monotonic for the three quantities (γ, R, A). The relative discrepancy between the fixed step-size solver with $\delta z = 0.001$ and the adaptive step-size solver, defined as

$$\text{discrepancy} = \left| \frac{\text{quantity}(\delta z = 0.001) - \text{quantity(adaptive)}}{\text{quantity(adaptive)}} \right|, \tag{28}$$

is less than 5×10^{-7} % for γ, less than 2×10^{-6} % for R, and less than 3×10^{-7} % for A. In the following, all computations are carried out by using the adaptive step-size Runge-Kutta solver.

DISCUSSION OF THE RESULTS

The onset of thermal instability in the porous channel is defined by the neutral stability curve drawn, for given values of (ξ, P), in the parametric plane (k, R). Even if the instability region is bounded from below by the neutral stability curve, it is the minimum of R versus k that defines the critical condition, (k_c, R_c), and thus identifies the critical mode which triggers the instability.
Figure 3 shows neutral stability curves for $P = 25, 50, 75, 100$. In each frame of this figure, different values of the form-drag parameter are considered, $\xi = 0, 10^{-3}, 5 \times 10^{-3}, 10^{-2}$. The case $\xi = 0$ offers a comparison with the behaviour observed in Darcy's flow regime, and analysed by Barletta (2012). We note that the discrepancy between the cases $\xi = 0$ and $\xi = 10^{-3}$ is not very large and gradually decreases as P decreases. In general, we observe a smaller influence of the form-drag parameter on the neutral stability curves as P becomes smaller. This trend is what could be reasonably expected, since the correction term affects the bulk flow with a contribution of order ξP. The already declared stabilising effect of the form-drag term is evident in Fig. 3, even if the neutral stability curves for $P = 25$ and different ξ may intersect at smaller values of k. The physical interest of this behaviour is minor, as the intersections occur with values of R above the critical threshold, $R > R_c$. Thus, the intersections belong to a supercritical domain, and as such they are unlikely to be revealed in an experiment where a natural perturbation is a superposition of all possible wavenumbers including the critical one, k_c. Figure 3 also displays comparisons, for each ξ and P, between the actual neutral stability curve (solid lines) and that obtained by claiming the asymptotic behaviour for $P \gg 1$ in agreement with Eq. (25). If the agreement is excellent when $P = 100$ and also when $P = 75$, discrepancies start to be visible when $P = 50$ and they

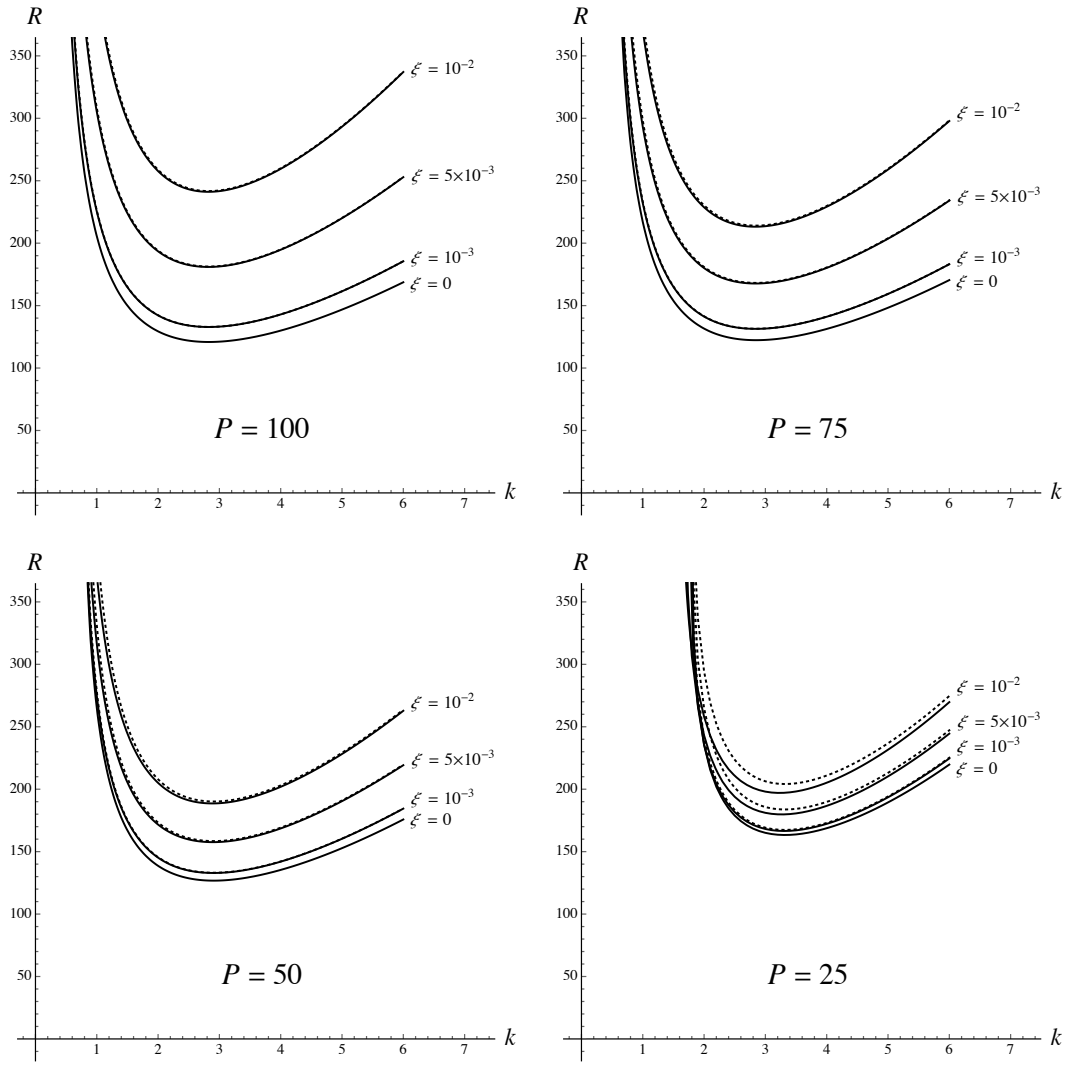

Figure 3. Longitudinal modes: neutral stability curves for different values of P and ξ. The dotted lines correspond to the asymptotic solution with $P \gg 1$ given by Eq. (25)

become even more pronounced when $P = 25$. Moreover, for a given ξ, the discrepancy is stronger the larger is ξ. The latter feature is an obvious fact since the curve $R_0(k)$, employed in order to apply the scaling given by Eq. (25), is obtained by a numerical solution for Darcy's flow ($\xi = 0$) and for a given P. In practice, we may say that the asymptotic scaling, Eq. (25), catches the main features of the form-drag effect as long as $P > 50$.

The stabilising role of the form-drag effect is actually reversed when the Péclet number becomes sufficiently small. An important feature of the neutral stability curves for smaller values of P, investigated for the regime of Darcy's flow by Barletta (2012), is that they assume a closed-loop shape. We mention that a closed-loop neutral stability curve means an island of instability surrounded by an unbounded region of stability. The closed-loops gradually shrink as P decreases until they collapse to a point when $P = 19.1971$ and eventually disappear (Barletta, 2012). Figure 4 is relative to $P = 19.22$. It is evident from this figure a generally destabilising role of the form-drag effect. Strictly speaking, this trend is inverted when ξ changes from 5×10^{-3} to 10^{-2}, as R_c in the former case is slightly smaller than in the latter case. We recall that, as specified in our analysis of the basic flow, we restrict the computation to parametric cases such that $A > 2R/P$, namely to the regime of unidirectional basic flow: $U(z) > 0$ for every $z \in [0, 1]$. Thus, we have drawn the neutral stability data limiting the plot range to this regime.

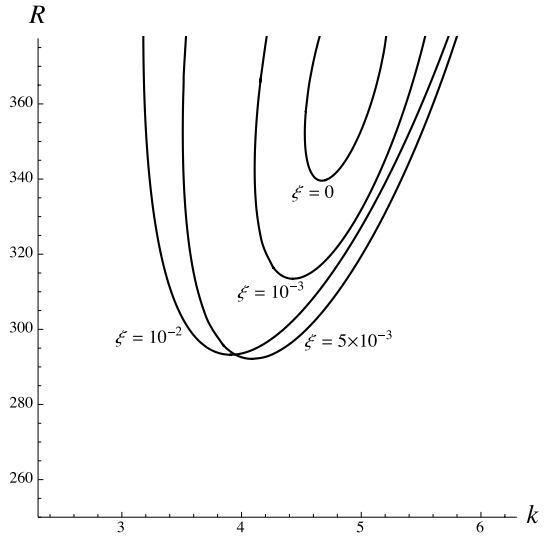

Figure 4. Longitudinal modes: neutral stability curves for $P = 19.22$ and different values of ξ

The neutral stability curves for the different values of ξ are expected to display a closed-loop shape on a larger range of Rayleigh numbers, exactly as in the limiting case $\xi \to 0$ (Barletta, 2012), even if this feature is not displayed in Fig. 4. Eventually, these closed loops are expected to shrink to a point, when P approaches its lower bound.

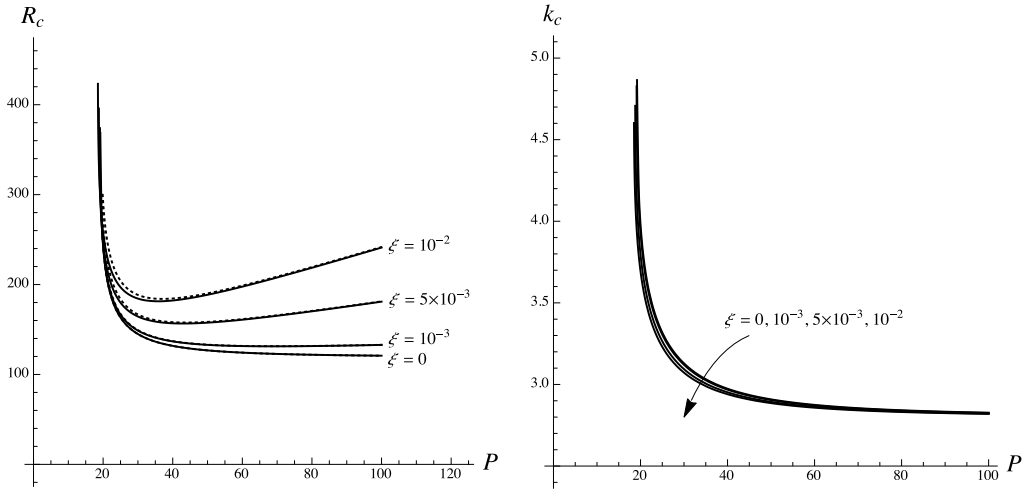

Figure 5. Longitudinal modes: critical values of R and k versus P, with different ξ. The dotted lines correspond to the asymptotic solution for $P \gg 1$ given by Eq. (25)

The critical values of R and k are plotted versus P in Fig. 5 for different values of the form-drag parameter, ξ. The general trend of R_c as a function of P shows a very steep increase as P becomes slightly smaller than 20. We also note the intersections among the plots of R_c versus P, in this range of small Péclet numbers. They actually reflect the already pointed-out switch between stabilising effect of ξ at larger Péclet numbers and destabilising effect at smaller values of P. We already mentioned that, when P is sufficiently large, the scaling induced by the form-drag effect and given by Eq. (25) yields a fairly good description of the neutral stability condition. This feature is confirmed by Fig. 5 both with respect to the plots of R_c versus P and to those of k_c. In particular, the plots of k_c are so weakly dependent on ξ that they fit the trend expected from Eq. (25), *viz.* a value of k_c not affected by ξ. On the other hand, the

dotted lines (asymptotic solution) are in good agreement with the plots of R_c versus P except for large values of ξ and for a limited range of Peclét numbers.

CONCLUSIONS

The mixed convection flow in a horizontal parallel channel filled with a porous material has been studied by including the form-drag effect in the local momentum balance equation (Darcy-Forchheimer's law). The walls of the channel have been modelled as impermeable and uniformly heated with symmetric uniform fluxes. The stability of the steady-state parallel flow has been studied with a linear analysis of perturbations. The analysis has been restricted to longitudinal modes. In fact, this kind of normal mode perturbations turned out to be the most unstable in a previous analysis of the same setup (Barletta, 2012) investigated according to Darcy's law and, hence, neglecting the form-drag effect.
The eigenvalue stability problem has been solved numerically by a combined procedure involving an explicit Runge-Kutta solver and the shooting method.
Three dimensionless parameters govern the basic parallel flow and its transition to convective instability: the Darcy-Rayleigh number R, the Péclet number P, and the form-drag parameter ξ.
The form-drag contribution to momentum balance has a stabilising effect when P is large enough, while its effect turns to destabilising at smaller values of P. A simple scaling law, with factor $\xi P + 1$, has been proved for the neutral stability values of R.

ACKNOWLEDGEMENTS

This research has been financially supported by Alma Mater Studiorum Università di Bologna with a FARB-FIBRA grant.

REFERENCES

Barletta, A. [2012], Thermal instability in a horizontal porous channel with horizontal through flow and symmetric wall heat fluxes, *Transport Porous Med.*, Vol. 92, pp. 419-437.

Barletta, A. [2013], Instability of mixed convection in a vertical porous channel with uniform wall heat flux, *Phys. Fluids*, Vol. 25, n. 084108.

Barletta, A., Celli, M. and Kuznetsov, A.V. [2013], Convective instability of the Darcy flow in a horizontal layer with symmetric wall heat fluxes and local thermal nonequilibrium, *ASME J. Heat Trans.*, Vol. 136, n. 012601.

Dodgson, E., Rees, D.A.S. [2013], The onset of Prandtl-Darcy-Prats convection in a horizontal porous layer, *Transport Porous Med.*, Vol. 99, pp. 175-189.

Nield, D.A. and Bejan, A. [2013], *Convection in Porous Media*, 4th ed., Springer-Verlag, New York, NY.

Prats, M. [1966], The effect of horizontal fluid flow on thermally induced convection currents in porous mediums, *J. Geophys. Res.*, Vol. 71, pp. 4835-4838.

Rees, D.A.S. [1997], The effect of inertia on the onset of mixed convection in a porous layer heated from below, *Int. Commun. Heat Mass*, Vol. 24, pp. 277–283.

Rees, D.A.S., Mojtabi, A. [2013], The effect of conducting boundaries on Lapwood-Prats convection, *Int. J. Heat Mass Tran.*, Vol. 65, pp. 765-778.